Earth Planet. Sci. Lett. 648 (2024) 119070

Contents lists available at ScienceDirect

Earth and Planetary Science Letters

journal homepage: www.elsevier.com/locate/epsl

Quantifying the loss of continental crust into the mantle from volume/mass balance calculations in modern collisional mountains

Ziyi Zhu [a,*], Zefeng Li [b], Ian H. Campbell [c], Peter A. Cawood [a], Neng Lu [c], Oliver Nebel [a,d]

[a] School of Earth, Atmosphere & Environment, Monash University, Melbourne, VIC 3800, Australia
[b] Research School of Astronomy & Astrophysics, Australian National University, Canberra, ACT 2611, Australia
[c] Research School of Earth Sciences, Australian National University, Canberra, ACT 0200, Australia
[d] GEOMAR Helmholtz Centre for Oceanic Research, 24148 Kiel, Germany

ARTICLE INFO

Keywords:
Crustal recycling
Mountain-building processes
Mass-balance calculations
Delamination

ABSTRACT

Reworking and recycling of continental crust, through processes such as erosion and delamination, are essential geological mechanisms that not only shape the topography of continents but also influence the composition of the continental crust and mantle. Continent-continent collisions are crucial settings to study these processes, as they primarily involve the thickening and uplift of the existing crust, with little new crustal addition compared with ocean-continent convergent plate boundaries. In this study, we investigate the three modern collisional systems that formed the Himalaya-Tibetan Plateau, the European Alps, and Zagros in central Asia, and quantify the amount of crust lost into the mantle by comparing the shortened crustal volume with the present-day preserved thickened crust, laterally extruded crust and surficial eroded crust. We find that crustal loss into the mantle accounts for at least 30% of the shortened crust, which exceeds the crust lost by surficial erosion by at least a factor of 2 in the Himalaya-Tibetan Plateau and Zagros. The volume of crust lost into the mantle during the formation of the Alps lies between 15% and 50%, depending on the values assumed for the pre-collisional crustal thickness and the volume of eroded crust.

For the Himalaya-Tibetan Plateau, our calculated crustal loss corresponds to an elevation increase of ~ 2 km, which can be explained by delamination of thick, eclogitised lower crustal roots in the late Oligocene, consistent with the distribution of shoshonitic-adakitic magmatism in southern Lhasa. This phase of rapid uplift, which followed the removal of dense lower lithosphere, corresponds with monsoon intensification in southern Asia. Furthermore, extending the concept of crustal loss to ancient mountain belts that occurred during the past cycles of supermountain formation, we propose that detachment of lower crustal roots can explain the trace element and isotopic characteristics of exotic crustal components in some plume-related mantle melts, ultimately linking mountain-building and mantle heterogeneity on a multi-million-year timescale.

1. Introduction

Recycling continental crust (CC) into the mantle has long been known to be a crucial geological process that has significantly influenced the time-integrated composition of the CC and the long-term evolution of the mantle (Cawood et al., 2013; White, 2015). A key mechanism for crustal recycling is the delamination and sinking of the lowermost crust into the underlying mantle, driven by the density increase due to the gabbro-eclogite transition, following lithospheric thickening at convergent margins (Lustrino, 2005). Delamination and detachment of lower lithosphere were initially proposed to explain the rapid uplift associated with igneous activity in the Colorado Plateau (Bird, 1979), the Southern Puna Plateau in the central Andes (Kay and Kay, 1993), and the Himalaya-Tibetan Plateau (England and Houseman, 1989). Loss of mafic lower crustal material has also been used to account for the intermediate composition of the bulk CC (Rudnick, 1995). Finally, it has been suggested that lost lower CC could melt and react with the surrounding mantle, leading to the compositional heterogeneity in Earth's mantle (Lustrino, 2005; Willbold and Stracke, 2010).

Loss of lower CC into the mantle can explain several geological observations. Qualitative evidence for the lower crustal loss includes rapid uplift (England and Houseman, 1989), low seismic velocity zones in the mantle (Bird, 1979), and geochemical signatures such as high La/Yb ratios, lack of Eu anomalies, and high Sr contents of magmas from the

* Corresponding author.
E-mail address: ziyi.zhu@monash.edu (Z. Zhu).

https://doi.org/10.1016/j.epsl.2024.119070
Received 29 June 2024; Received in revised form 2 October 2024; Accepted 9 October 2024
Available online 24 October 2024

base of tectonically thickened crust (Kay and Kay, 1991). Mass-balance calculations provide a quantitative tool to evaluate the input of CC into the mantle (Ingalls et al., 2016; Replumaz et al., 2010).

In this study, we establish and apply volume/mass balance equations to quantify the amount of CC returned to the mantle during continent-continent collisions. We consider three modern mountain ranges for which the required data to assess such a quantification are available: the Himalaya-Tibetan Plateau, the European Alps and the Zagros Mountains. These mountains formed at different times during the Cenozoic, with critical parameters, such as initial crustal thickness and crustal shortening estimates, being better constrained than for older mountain belts. Our calculations agree with previous studies of the Himalaya-Tibetan Plateau, which show that the crustal mass budget cannot be balanced during the India-Asia collision (Ingalls et al., 2016; Replumaz et al., 2010) without the return of material to the mantle. We attribute this imbalance to the loss of dense lower CC from the mountain roots via delamination, which is defined as rapid foundering or detachment of the lower lithosphere. We find that this imbalance persists in the collisions that formed the Alps and Zagros mountains.

2. Methods

This section provides a theoretical basis for the crustal volume/mass balance equations for continent-continent collisions used in this study. We envision a simple mountain-building model, in which the collision occurs along a boundary of a constant length L_{sh} between two crustal blocks with an initial crustal thickness of c (Fig. 1). The total volume of the shortened crustal block (V_{sh}) can be calculated from

$$V_{sh} = L_{sh} c D_{sh} = L_{sh} c \int_0^T v(t)dt \tag{1}$$

where D_{sh} is the total shortened distance, which is the integral of convergence rate (v) over the time (T) to form the orogen.

In Fig. 1, the thickened crust refers to the excess crustal material relative to the initial crustal block with a normal crustal thickness of c. Assuming that the mountain belt forms along the collisional boundary of a constant length (L_{sh}) and has a constant width of w, we can calculate the volume of thickened crust without the initial crustal block (V_{th}) as follows:

$$V_{th} = L_{sh} w(\overline{H} - c) \tag{2}$$

where $\overline{H}$ is the total crustal thickness from the surface to the Moho.

Alternatively, the volume of the thickened crust can be calculated by adding the volume of the topography above normal, unthickened crust (V_{topo}), to the volume of the mountain root below the unthickened crust (V_{root}), which is expressed as

$$V_{th} = V_{topo} + V_{root} \tag{3}$$

or

$$V_{th} = L_{sh} w(\overline{h} + \overline{r}) \tag{4}$$

where $\overline{h}$ and $\overline{r}$ represent the average height of the mountain and depth of its root, relative to the top and bottom of the unthickened crust, respectively. Both increase proportionally as the crust thickens.

In a normal crust above sea level (Fig. S1), the correlation between $\overline{h}$ and $\overline{r}$ is controlled by the average densities of crust (ρ_c) and mantle (ρ_m), assuming a simple Airy-type isostatic model, in which the isostatic balance is assumed to occur at the base of the crust:

$$\overline{r} = \frac{\rho_c}{\rho_m - \rho_c}\overline{h} \tag{5}$$

This relationship is based on the balance of buoyancy forces that lift the low-density crustal blocks above the high-density mantle, and gravity forces that pull the crustal blocks downwards (Kearey et al., 2009). Eqs. (4) and (5) can be combined to obtain an expression for the volume of thickened crust as follows:

$$V_{th} = \frac{\rho_m}{\rho_m - \rho_c} L_{sh} w \overline{h} \tag{6}$$

We denote $\frac{\rho_m}{\rho_m - \rho_c}$ by r_ρ. Estimates of the average density of crust ρ_c range from 2.75 g/cm^3 to 2.87 g/cm^3 (Gvirtzman et al., 2016; Lee et al., 2015; McKenzie and Priestley, 2016), and typical mantle densities from 3.30 g/cm^3 to 3.33 g/cm^3 (Lee et al., 2015; McKenzie and Priestley, 2016). These values give a typical density contrast between crust and mantle of 0.43–0.58 g/cm^3, resulting in r_ρ values in the range of 5.7–7.7.

Eq. (5) shows that, if the crust is in Airy isostatic equilibrium, variations in elevation are determined by variations in crustal thickness, which is expressed as

$$\frac{d\overline{h}}{d\overline{H}} = 1 - \frac{\rho_c}{\rho_m} \tag{7}$$

However, the weak correlation between the global topography and crustal thickness data suggests that the commonly used Airy-type isostasy model is insufficient to explain the topography of crustal regions on a global scale (Gvirtzman et al., 2016). Specifically, it fails to explain the topography for regions with a crustal thickness ranging from approximately 25 km to 50 km (Lamb et al., 2020). In contrast, the Airy-type model gives good results for crust thickness greater than 50 km (Gvirtzman et al., 2016). This observation is consistent with the study by Lee et al. (2015), who found a positive correlation between elevation and crustal thickness for mountain belts with an elevation greater than 2 km, corresponding to crustal thicknesses greater than 48 km, based on an initial crustal thickness of 35 km and r_ρ of 6.7. Furthermore, the positive correlation remains if data from Zagros and Alps are added to the original plot of Lee et al. (2015), which includes data from the Tibetan Plateau, Andes and Rocky Mountains (Fig. S2). Therefore, we conclude that the Airy-type isostatic model gives acceptable estimates of the elevation of high mountain ranges ($>$ 2 km), but not for thin crust.

The formation of high mountains is accompanied by elevated rates of weathering and erosion, producing large amounts of sediments that are delivered to the oceans by rivers. For example, the Himalayan orogen, which has the highest topographic relief, has produced the two largest sedimentary fans on Earth – the Bengal and Indus fans. The Bengal Fan has a volume of 12.5×10^6 km^3, making it approximately twenty times larger than the Amazon fan and forty times larger than the Mississippi fan (Curray et al., 2002). The volume of crust lost through erosion ($V_{erosion}$) can be constrained by the reported sediment data from the literature.

Finally, it is possible that the vertical thickening of the crust is accompanied by the movement of the crust in a direction oblique to the direction of thickening and shortening (Fig. 1D). In some delineations of mountains, such as the modern Alps and Zagros as discussed below, the length of the mountain L includes the lateral displacement of CC (ΔL). This displacement of CC is defined as crustal lateral extrusion. The volume of extruded material is given by

$$V_{extrusion} = \Delta L w \overline{H} \tag{8}$$

3. Results

We apply the equations outlined above to three modern mountains produced by continent-continent collisions: the Himalaya-Tibetan Plateau, Alps and Zagros. Applying the theoretical model of Fig. 1 to real-world scenarios is challenging due to uncertainties in the essential parameters and requires significant simplification. We provide plausible justifications for the parameters based on geological evidence. We first assume that the vertical variation in the density of CC can be neglected, and evaluate if V_{sh} is balanced by V_{th}, $V_{erosion}$ and $V_{extrusion}$, using

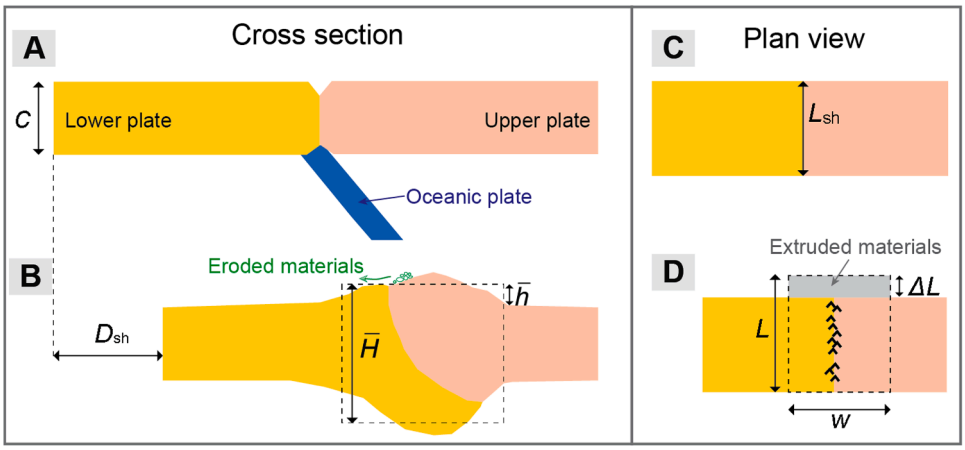

Fig. 1. Conceptual cross-sections and plan views showing the horizontal shortening of continental crust, with an initial crustal thickness of c (A), along a boundary with a length of L_{sh} (C), is accommodated by the vertically thickened crust (B), which comprises a mountain belt with a high elevation above the surface and a thick mountain root, the eroded materials, and the continent block that is extruded orthogonal to the shortening direction (D). This figure is not to scale because the depth of the root is around six times greater than the height of the mountain in a simple Airy-type isostatic model. The total shortened distance (D_{sh}) is the sum of the shortening in the two colliding blocks. $\bar{H}$ is the total thickness of the crust within the orogen, whereas $\bar{h}$ and w are the average height and width of the mountain belt, respectively. In some cases, such as the modern Alps and Zagros, the length of the mountain L includes both the length of the collision zone along which the continental crust was shortened (L_{sh}), and the movement distance of the extruded crustal block (ΔL) within the mountain region.

parameters including average mountain length (L), width (w), height ($\bar{h}$) and total crustal thickness ($\bar{H}$)[1]. We then consider a simple density profile for the eclogitic crust below 45 km depth, crust above 45 km depth and sediments, and examine if the crustal mass is conserved. The shapes of mountain ranges are from Natural Earth's physical vectors (Fig. 2).

3.1. Calculating shortened crust

3.1.1. Himalaya-Tibetan Plateau

Despite decades of studies on the Himalaya-Tibetan Plateau, the convergence history of India-Asia and the nature of the Indian margin before the collision remain controversial (Ding et al., 2022; Parsons et al., 2020). The onset of the India-Asia collision was dated at ca. 59 Ma by the first deposition of Asia-derived detritus onto the distal edge of India (Hu et al., 2016). However, the suturing between India and Asia along a long (~1000 km) belt was not completed until ca. 50 Ma (Ingalls et al., 2016). This is consistent with the cessation of marine sedimentation in many places along the Tethyan Himalaya margin and a reduction in the India-Asia convergence rate from around 16 cm/yr to 8 cm/yr at 50 Ma (Hu et al., 2016; van Hinsbergen et al., 2011). Since the initial collision, plate reconstruction indicates that the total convergence between India and Asia was about 3000 km (Van Hinsbergen et al., 2012). However, only 1000–2000 km of the convergence can be accommodated by bed-rock crustal shortening estimates (Van Hinsbergen et al., 2012). To account for the difference between the convergence and the preserved shortening, some researchers argue the existence of a 1000–2000-km-wide portion of continental margin, termed Greater India, which was subducted/delaminated into the mantle without being preserved in the surficial bedrock record (Hu et al., 2016; Ingalls et al., 2016), whereas two other groups suggest the existence of the Neo-tethyan oceanic lithosphere (Aitchison et al., 2007) or the Greater India basin (Van Hinsbergen et al., 2012) before the hard India-Asia collision began at ca. 35 Ma and 25–20 Ma, respectively. Among the three hypotheses, the model of an enlarged Greater India continental crust, since the Eocene, is most consistent with the available bedrock records and geophysical observations (Parsons et al., 2020), whereas the latter two are met with challenges such as the inconsistencies with some seismic tomography models and lack of evidence for the suture zone that corresponds to the closure of the oceanic basin (Hu et al., 2016; Parsons et al., 2020).

The analytical model of Guillot et al. (2003) is used to reconstruct the convergence distances (D_{sh}) for Asian and Indian continental blocks from 50 Ma to the present, which are estimated to be 1115 and 1632 km, respectively. Note that here the Indian convergence consists of 1010 km of Himalayan shortening (displacement of India relative to the southern Indus Suture Zone) and 622 km of the hypothetical Greater India continental margin (Fig. 2). The estimate of D_{sh} for Asia is multiplied by an initial crustal thickness (c) of 32–35 km, which is the range of the present-day crustal thickness of the unthickened Asian continent (Replumaz et al., 2010). This is a conservative estimate since part of the southern Asian plate, including the Gangdese magmatic arc belt, was probably thickened to > 50 km at 55–45 Ma (Zhu et al., 2017). For the Indian continent, c is estimated to be 35–40 km for the Himalayan block, based on the thickness of the present-day undeformed Indian continent (Replumaz et al., 2010), and 26 km for Greater India, which is the average thickness of continental margins worldwide (Mooney et al., 2023). The results of V_{sh} calculated by these values of D_{sh} and c are shown in Supplementary Table1.

3.1.2. Alps

The European Alpine orogeny began when the European continental margin entered the subduction zone adjacent to the Adria indenter around 35 Ma, coinciding with a decrease in the Europe-Adria convergence rate from 1.5 cm/yr to <1.3 cm/yr (Handy et al., 2010). At this time, the Alpine foreland basin on the European margin was characterised by marine underfilled flysch, consisting of alternating turbiditic flysch and mudstone (Sinclair, 1997). This was followed by the overfilled terrestrial molasse sedimentation from ca. 30 Ma, indicating a transition to a continental environment (Schlunegger and Kissling, 2022). This stratigraphic progression suggests that, by 30 Ma, the shortening of the European crust had begun, with a normal thickness ranging from 28 km to 32 km, based on the crustal thickness of post-Variscan regions of Central and Western Europe (Giese, 2005). Between 35 and 30 Ma, the European continental margin experienced a maximum shortening of 65 km, based on a Europe-Adria convergence rate of 1.3 cm/yr. For the Adriatic continent, the initial crustal thickness

[1] The details of constraining these parameters are presented in Supplementary Material, and the source codes for the calculations are provided in the GitHub website.

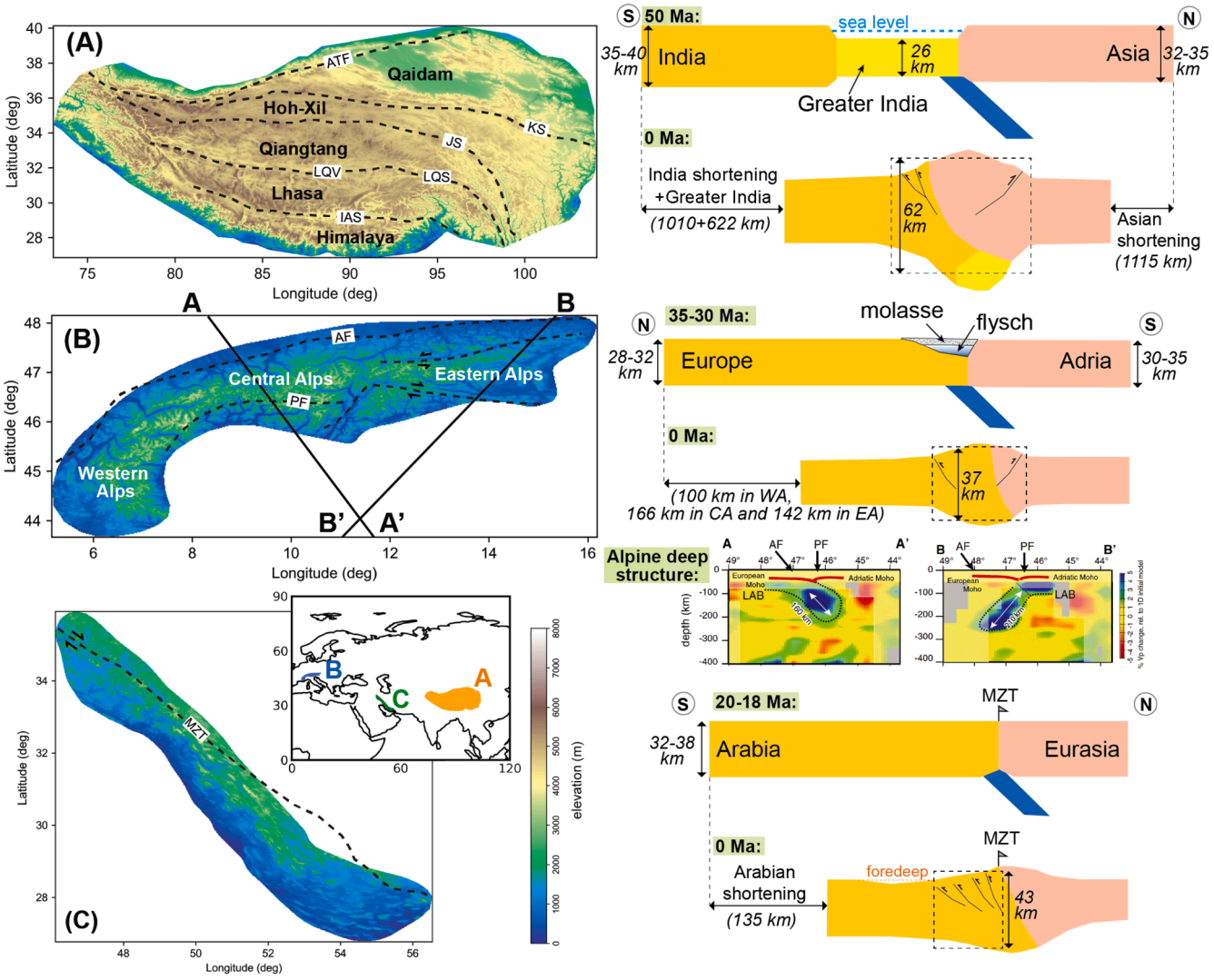

Fig. 2. Mountain ranges of the (A) Himalaya-Tibetan Plateau, (B) Alps and (C) Zagros, from Natural Earth's physical vectors. The inset in the last panel shows the locations of these mountain ranges. The elevation data in metres above sea level are from ETOPO1 (Amante and Eakins, 2009). Major tectonic lineaments are from Ding et al. (2022), Sánchez et al. (2018) and Su and Zhou (2020). Abbreviations: AF, Alpine Front; ATF, Altyn Tagh fault; IAS, India-Asia suture; JS, Jinsha suture; KS, Kunlun suture; LQS, Lhasa-Qiangtang suture; LQV, Lhasa-Qiangtang suture valley; MZT, Main Zagros Thrust; PF, Periadriatic fault. The conceptual cross-sections on the right illustrate our constraints on the initial crustal thicknesses and shortening distances used to calculate V_{sh} (refer to Section 3.1 for details). The deep seismic structure in the Alpine region is from Lippitsch et al. (2003).

is estimated to be 30–35 km, based on the measured Moho depth for the Adriatic foreland from several seismic models (Giese, 2005; Zhang et al., 2022).

The estimated post-collisional shortening since 35 Ma is at least 80–120 km in the Western Alps, 126–206 km in the Central Alps, and 125–159 km in the Eastern Alps (Kästle et al., 2020 and references therein). We thus assign an average total shortening (D_{sh}) of 100 km in the Western Alps, 166 km in the Central Alps, and 142 km in the Eastern Alps (Fig. 2). These estimates are then multiplied by the average initial crustal thickness of Europe and Adria, ranging from 29 to 33.5 km, except for the first 65 km of convergence, where a thickness of 26 km is used for the continental margin. In the Eastern Alps, the north-south shortening was accompanied by the formation of large strike-slip faults that facilitated the eastward extrusion of crustal blocks. Restoration of fault displacements indicates the 120 km east-west lateral movement of the central Eastern Alps in the Miocene (Linzer et al., 2002). Before this movement, the length of the collision zone, along which the CC was shortened, was therefore equal to the length of the present-day orogen boundary minus 120 km. This adjusted length is used to calculate V_{sh} for the Alps (Supplementary Table1).

3.1.3. Zagros

The Zagros Mountains formed by the Arabia-Eurasia collision, beginning at ca. 35 Ma (Mouthereau et al., 2012). However, the onset of collision between Eurasia and Arabia crust with a normal thickness, likely occurred later at ca. 20–18 Ma, as supported by rapid exhumation and intensive thrusting in the High Zagros from ca. 19 Ma (Gavillot et al., 2010), and a reduction in Arabia's plate velocity at ca. 20 Ma (Hatzfeld and Molnar, 2010). This is consistent with the deposition of the ca. 20–18 Ma Asmari limestone overlain by the Gachsaran evaporitic deposits and the Agha Jari fluvial deposits in the northwest and central Zagros, indicating a transition from a marine to nonmarine environment (Mouthereau et al., 2012; Pirouz et al., 2017a). Therefore, we assume that the initial crustal thickness of the Arabian crust, since the start of the hard collision, was at least 32 km, which is the average crustal thickness at sea level (Lamb et al., 2020). The local reference crustal thickness of 38 km for an isostatically balanced crust with zero topography, as determined by Pirouz et al. (2017a) based on the free-air anomaly and seismological constraints, is used as a maximum choice for c. This range of 32–38 km is consistent with the crustal thickness of the present-day undeformed Arabian plate measured by regional

geophysical studies (Blanchette et al., 2020).

The Zagros region that we use here (Fig. 2) is bounded to the north by the Main Zagros Thrust (MZT), which represents the plate boundary between Arabia and Eurasia. Therefore, only D_{sh} on the Arabian side is considered when calculating V_{sh}. We adopt D_{sh} of 135 km in central Zagros since the early Miocene (Mouthereau et al., 2012), which includes a shortening of 15 km that is accommodated in the Zagros Folded Belt and 120 km in the High Zagros. This is consistent with the estimates of 152 ± 30 km for shortening in the Arabian plate since ca. 18 Ma based on restored cross sections (Su and Zhou, 2020), 135 km based on flexural modelling (Pirouz et al., 2017b), and 100–155 km based on structural studies (McQuarrie and van Hinsbergen, 2013). In the northern Zagros, there is a $\sim$ 50 km displacement along the dextral Main Recent Fault (Talebian and Jackson, 2002). This displacement distance, together with the postulated length of the shortened crust (L_{sh}), makes up the present-day length of the mountain. The results of V_{sh}, based on this L_{sh} and c of 32–38 km are provided in Supplementary Table1.

3.2. Calculating thickened crust

V_{th} is computed by subtracting the initial crustal block, with a crustal thickness of c, from the present-day crust with a total crustal thickness of $\overline{H}$. This is named the Moho method since it relies on Moho depth data from the CRUST1.0 model (Laske et al., 2013). We also provide results for V_{th}, calculated by the Airy method for comparison, using the average mountain height $\overline{h}$. However, as discussed earlier, the Airy-type isostatic model is less reliable, especially when applied to thin crust. The results of V_{th_moho} and V_{th_airy} for the Himalaya-Tibetan Plateau (Supplementary Table1) are similar, which suggests that the crust is in Airy isostatic equilibrium.

3.3. Estimating eroded crust

The volume of lost crust through surficial erosion is taken from literature data. For the Himalaya-Tibetan Plateau, $V_{erosion}$ is estimated to be the total volume of the Bengal Fan, Indus Fan, Himalayan foreland, Tarim and south-eastern Asian basins, which is 27×10^6 km^3 (Clift et al., 2009). The estimated total amount of sediment derived from the Alps ranges from 0.51×10^6 km^3 (Clift et al., 2009), based on the volume of foreland, Po Valley, Pannonian Basin, Rhone delta and Danube delta, to 0.87×10^6 km^3 (Kuhlemann et al., 2001), calculated using the sediment budget and thermochronological data. These two estimates are used as the minimum and maximum values of $V_{erosion}$ for the Alps. The eroded material in the Zagros Mountains, derived from the thickened crust, is now stored in the post-Asmari foreland fill and estimated to be 0.57×10^6 km^3 (Pirouz et al., 2017a). Using these estimates, the volume of eroded crust accounts for $<$ 20% of the shortened crust in the three examined orogens (Fig. 3). For comparison, in Supplementary Material, we provide a theoretical estimate of $V_{erosion}$ based on the relationship between erosion rate and relief, as proposed by Vance et al. (2003).

3.4. Estimating extruded crust

During the India-Asia convergence, a large volume of the Asian CC was extruded eastward from central Tibet towards Indochina (Leloup et al., 1995). The volume of the crustal material that was transported outside the deformed Asian domain is estimated by Ingalls et al. (2016) to be $(15.5 \pm 8.5)\times10^6$ km^3, and this is taken as our estimate of $V_{extrusion}$ for the Himalaya-Tibetan orogen. The extruded block is included in the present-day mountain domains for the Alps and Zagros mountains. $V_{extrusion}$ for these orogens is calculated by multiplying the width of mountain belts (w), total crustal thickness ($\overline{H}$) and the displacement values for the CC (ΔL) as suggested above.

3.5. Defining orogenic loss

There is a discrepancy between V_{sh} and the sum of V_{th}, $V_{erosion}$, and $V_{extrusion}$ for the three modern orogens (Fig. 3). The concept of orogenic loss, denoted as Δ_{oro}, is introduced to represent the percentage of shortened CC that cannot be accounted for in the crust materials preserved above the Moho. It is defined by

$$\Delta_{oro} = \left(1 - \frac{V_{th} + V_{erosion} + V_{extrusion}}{V_{sh}}\right) \times 100\% \quad (9)$$

Our preferred results for Δ_{oro} are based on V_{th_moho}, whereas the less reliable results using V_{th_airy} are provided in Fig. S3 for comparison.

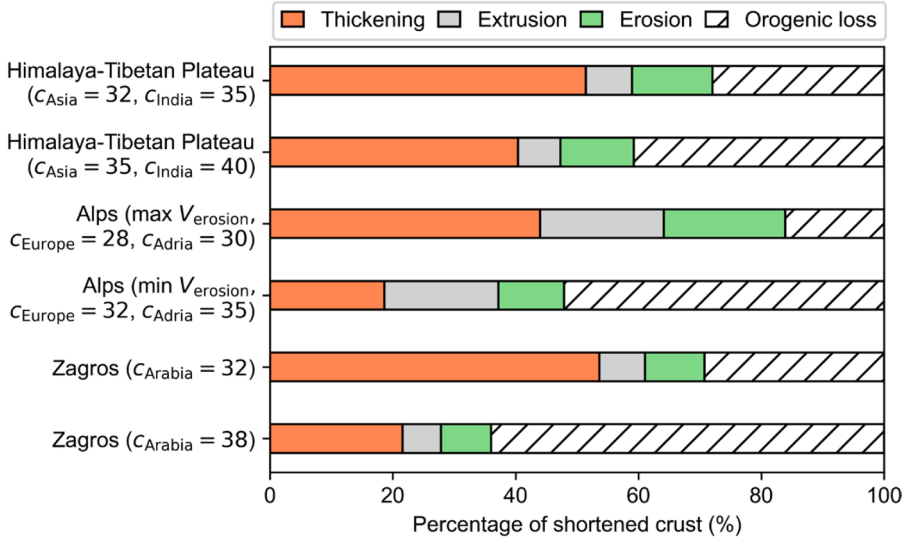

Fig. 3. Horizontal bar plots showing the distribution, by volume, of crustal thickening, extrusion, erosion, and orogenic loss for the Himalaya-Tibetan Plateau, Alps, and Zagros. The bars represent the percentage of each category contributing to the overall crustal shortening in these regions. Here the minimum and maximum estimates of initial crustal thickness (c, in the unit of kilometres) give the lower and upper boundaries of orogenic loss, which represents the percentage of shortened crust unaccounted for by thickening, erosion, and extrusion. The results for the Alps also consider minimum and maximum estimates of $V_{erosion}$, which are 0.51×10^6 km^3 (Clift et al., 2009) and 0.87×10^6 km^3 (Kuhlemann et al., 2001), respectively. The volume of the thickened crust, which refers to the additional crust added by the collision excluding the initial crustal block, is calculated based on Moho depth data.

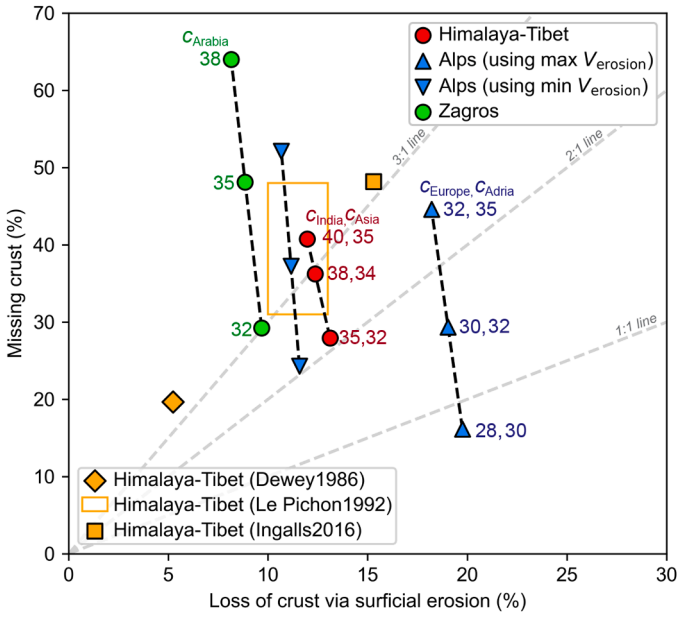

Fig. 4. Scatter plot for the percentage of missing crust unaccounted for by thickening, erosion and extrusion, i.e., orogenic loss, versus eroded crust in the overall crustal shortening for the Himalaya-Tibetan Plateau, Alps, and Zagros. The values in kilometres, displayed near each data point, represent different initial crustal thicknesses used in the calculations. For the Alps, the results also account for minimum and maximum estimates of $V_{erosion}$, which are 0.51×10^6 km^3 (Clift et al., 2009) and 0.87×10^6 km^3 (Kuhlemann et al., 2001), respectively. For the Himalaya-Tibetan region, the results are compared with three previous studies: Dewey et al. (1986) based on cross-sectional area estimates, Le Pichon et al. (1992) on surficial area estimates (box representing a range), and Ingalls et al. (2016) on 3D mass balance estimates (Supplementary Table 2). Dewey et al. (1986) and Le Pichon et al. (1992) did not account for lateral extrusion in their calculations of missing crust. The dashed 1:1, 2:1 and 3:1 lines are for reference.

Fig. 4 shows that Δ_{oro} is at least ~ 30% for the Himalaya-Tibetan Plateau and Zagros, with Δ_{oro} greater than the crust lost by surficial erosion by at least a factor of 2. For the Alps, Δ_{oro} varies from around 15% to 50% using different estimates of c and $V_{erosion}$. Δ_{oro} exceeds 60% in the result of Zagros based on a c of 38 km. However, this is a potential overestimate since the thickened Arabian crust (V_{th}) may be an underestimate because seismic images show underthrusting of the Arabian crust beneath the Eurasian crust about 250 km in the northern Zagros and 140 km in the central Zagros Mountains (Paul et al., 2010). Since c of 32 km gives the minimum estimate of V_{sh} and thus minimum Δ_{oro}, we conclude that the orogenic loss for the Zagros Mountains is between 30% and 64%.

Finally, we calculated the orogenic mass loss by using a density of 3.3 g/cm^3 for garnet-bearing eclogitised crust beneath 45 km depth, 2.8 g/cm^3 for the crust above 45 km depth, and 2.25 g/cm^3 for the eroded sediments (Replumaz et al., 2010). The results for Δ_{oro}, based on mass, agree with those obtained from the volume (Supplementary Table1): approximately 20–50% of the mass of the CC was lost to the mantle during the formation of the Himalaya-Tibetan Plateau, Alps and Zagros mountains. The only possible exception is Zagros, which shows > 60% of the CC was lost if the value of 38 km is used for c.

4. Discussion

4.1. Is the orogenic loss hypothesis correct?

Several simplifications and assumptions are required in our model to calculate the orogenic loss during the complex evolution of an orogenic belt. These assumptions include (i) the collision boundary between the two continental crustal blocks has a constant length of L_{sh}, (ii) each mountain range can be approximated by a rectangle with a length of L and a width of w (Supplementary Material), and (iii) the mountain width w remains constant during the collision. These assumptions do not affect the estimates of $V_{erosion}$ or $V_{extrusion}$, which are independently constrained. They also have minimal effect on V_{th}, because using Eq. (2), together with our approximated L and w, provides an accurate estimation of mountain volume, which is the same as the integrated volume of all grid cells covering the mountain range (Supplementary Material). However, these assumptions, combined with various estimates of the shortened distances, since the collision, could potentially introduce large uncertainties in V_{sh}. Despite these limitations, our calculated V_{sh} for the Himalaya-Tibetan Plateau since 50 Ma, which is (206–226) $\times$ 10^6 km^3 based on the lower and upper bounds of the initial crustal thicknesses, agrees with (i) (200–217) $\times$ 10^6 km^3 based on the surficial area shortening of (57–62) $\times$ 10^5 km^2 since 45 Ma by Le Pichon et al. (1992) using an initial crustal thickness of 35 km, and (ii) 330 $\times$ 10^6 km^3 from Ingalls et al. (2016) obtained by multiplying the convergence area in different suture zones at different collision times with their respective initial thicknesses. We therefore conclude that our simplified mountain-building model provides a reasonable estimate of V_{sh}.

The 'missing crust' that cannot be accommodated by present-day crustal thickening, erosion or extrusion, i.e. Δ_{oro} as defined in this study, has been previously recognised for the Himalaya-Tibetan Plateau. Fig. 4 shows that the percentage of missing crust in the overall shortened crust in our study (28–41%) lies between the results of Dewey et al. (1986) based on a cross-sectional area estimate (20%), and Ingalls et al. (2016) based on a 3D mass balance estimate (48%). It also falls close to the range obtained by Le Pichon et al. (1992), based on a surficial area estimate since 45 Ma (31–48%). However, both Dewey et al. (1986) and Le Pichon et al. (1992) did not account for the influence of lateral extrusion in their calculations. As a consequence, if extrusion were considered in their studies, the orogenic loss would be slightly lower than the missing crust shown in Fig. 4. Although different methodologies are used in each of these previous studies, the similarity between our result and theirs suggests that the orogenic loss in the Himalaya-Tibetan Plateau is both real and significant.

Our calculations provide the first quantified evaluation of the orogenic loss in the Alps and Zagros based on the relative contribution of crustal thickening, erosion and extrusion in shortening (Figs. 3 and 4). The loss of CC into the mantle has been qualitatively described in previous studies of these regions. For instance, the southward-dipping slab at ~ 200 km depth, seen in tomographic images beneath the Central Alps (Fig. 2), has been widely interpreted as the subducted lower European lithosphere, since its down-dip size of 160 km corresponds roughly to the amount of post-collisional crustal shortening in the Alpine nappe stack (Lippitsch et al., 2003). Similarly, in the eastern Alps, the northward-dipping slab, between depths of 50 and 250 km, is interpreted as the continental subduction of Adria beneath Europe (Lippitsch et al., 2003), although a European origin for this slab has also been suggested (Kästle et al., 2020). In both cases, it has been proposed that the lower CC was subducted together with its lithospheric mantle as part of the down-going slab (Schmid et al., 1996), with its detachment from the upper crust potentially driven by the rheological and density differences. For the Zagros orogen, previous studies suggest that CC may have returned to the mantle through (i) the entrainment of continental passive margin with the detached oceanic lithosphere at ca. 10 Ma (Fig. S4A) (Darin and Umhoefer, 2022), (ii) subduction of eclogitised CC (Pirouz et al., 2017b), and/or (iii) lithospheric dripping (Hatzfeld and Molnar, 2010).

4.2. Possible mechanisms of orogenic loss in the Himalaya-Tibetan Plateau

Continental subduction and delamination are the two main hypotheses suggested for CC recycling of the Himalaya-Tibetan Plateau.

The former involves the decoupling of the upper crust from denser lower CC, which sinks with the subducting lithospheric mantle (Fig. S4B) (e.g., Ingalls et al., 2016), whereas the latter involves periodic detachment of the lower CC and underlying subcontinental lithospheric mantle (SCLM) (e.g., Chung et al., 2009). With a main focus on the consequences of the process, we define delamination in this paper as the rapid foundering or detachment of the lower lithosphere (SCLM and dense lower crust) into the asthenospheric mantle (Fig. S4C) (Kay and Kay, 1993; Lustrino, 2005), without specifying the mechanics and dynamics of delamination. The key difference here is that continental subduction is a continuous process of losing CC into the mantle, whereas delamination is episodic.

Ingalls et al. (2016) proposed that the eclogitic Indian lower crust was subducted into the upper mantle beneath southern Tibet. Their hypothesis is based on the combination of shallow and deep seismic evidence: P-wave tomography shows ongoing subduction of the Indian lithosphere below the Asia plate in the upper mantle at depths between 100 and 410 km (Li et al., 2008), whereas receiver function studies reveal the existence of a 19-km-thick layer of presumed eclogitised crust at ~ 60–80 km depth that extends northwards and is interpreted to be related to underplating of Indian lower crust beneath Tibet (Nábělek et al., 2009). The detachment of the lower CC from the upper crust and its subsequent subduction is supported by numerical modelling (Capitanio et al., 2010), although the feasibility of wholescale continental subduction is debated (van Hinsbergen et al., 2017). To account for the calculated orogenic loss of (58–92) $\times$ 10^6 km^3 in this study, the continental-subduction hypothesis requires a slab of lower CC with an average width (down-dip dimension) of 1293–2052 km and thickness of 19 km to be subducted along the 2360 km collisional boundary. Although this hypothetical width of 1293–2052 km exceeds the seismically imaged length of the continuous northwards downwelling India slab in the upper mantle (Li et al., 2008), part of the dense eclogitic lower crust may have detached from the subducted lithosphere and stagnated in the mantle transition zone (Parsons et al., 2020). However, current geophysical methods cannot distinguish between the deeply subducted CC and lithospheric mantle, and direct geological evidence for the continuous large-scale CC subduction is lacking.

Delamination of eclogitised lower crustal roots, which has been proposed to explain the formation of the Cenozoic shoshonitic (high-K) and adakitic (high-Sr and low-Y) rocks in southern Tibet (Campbell et al., 2014; Chung et al., 2009), supports the lower CC recycling hypothesis for the Himalaya-Tibetan Plateau. Delamination is driven by the high-pressure transformation of plagioclase to garnet in the mafic component of the lower CC to form eclogite with a density of 3.4–3.8 g/cm^3, which is higher than the upper mantle density of 3.3 g/cm^3. This density increase leads to gravitational instability of the over-thickened lithospheric keel, which sinks into the asthenosphere (Lustrino, 2005). The region vacated by the delaminated lithosphere may then be replaced by the hot asthenospheric mantle, which can provide the heat required to melt the sinking crustal portion of the delaminated material and the base of the CC. Partial melting of the source with a 'crustal' signature, such as enrichment in large ion lithophile elements, including K, then produces melts with high SiO_2 and high K_2O (shoshonitic). The high Rb/Sr ratio of the CC, and thus high time-integrated $^{87}Sr/^{86}Sr$, results in the observed high $^{87}Sr/^{86}Sr$ of shoshonitic melts (Campbell et al., 2014). The contemporary post-collisional adakites of Tibet, characterised by high Sr/Y and strong depletion in heavy rare earth elements, require the presence of garnets in the residue, consistent with their derivation at depths (Chung et al., 2009). The shoshonitic/adakitic melts derived from the sinking block will be out of equilibrium with olivine in the overlying mantle and will react with it during their ascent to produce orthopyroxene. This reaction lowers the SiO_2 content of the melt, which explains the spread of SiO_2 to lower values in some of the shoshonitic-adakitic rocks in Tibet (Campbell et al., 2014; Zeng et al., 2021).

Delamination is also expected to lead to a phase of rapid uplift due to the isostatic compensation after the hot asthenosphere replaces the cool, sinking dense material (Bird, 1979; England and Houseman, 1989; Kay and Kay, 1993). Assuming the loss of (58–92) $\times$ 10^6 km^3 of CC from the Himalaya-Tibetan Plateau, as calculated in this study, occurred through delamination, we can quantify the resultant elevation increase Δh based on a two-step approach. First, we determine the thickness of the delaminated crustal block ΔD (Fig. S5), using $Lw\Delta D = (58 \sim 92) \times 10^6$ km^3, where L and w represent the length and width of the orogen, respectively. The value obtained is 20.4 $\pm$ 4.7 km. We then calculate Δh from ΔD, since under a simple Airy-type isostatic model, their correlation is controlled by the average densities of eclogitised lower crustal root (ρ_{ec}) and mantle (ρ_m), which is expressed as $\Delta h = \frac{\rho_{ec}-\rho_m}{\rho_m}\Delta D$ (Supplementary Material). $\frac{\rho_{ec}-\rho_m}{\rho_m}$ ranges from 0.03 to 0.15, taking into account uncertainty in ρ_{ec} (3.4–3.8 g/cm^3) and ρ_m (3.3 g/cm^3) (Lustrino, 2005). The calculated value of Δh is 2.1 $\pm$ 1.6 km, which agrees with an elevation increase from 2–3 km at 24–23 Ma to 4–5 km at 20 Ma as shown in the compiled paleo-elevation record (Fig. 5B). In other words, the delamination of an average 20.4 km thick crustal block would result in the crustal volume imbalance calculated in this study and the ~ 2 km uplift observed in the late Oligocene from the paleo-elevation record (Ding et al., 2022). The formation of widespread potassic-adakitic magmatism in the Lhasa terrane since the late Oligocene (Fig. 5A), further supports the occurrence of a delamination event at that time. Interestingly, Fig. 5B shows a rapid subsidence of 2 km within 2 Myr before the late-Oligocene rapid uplift. Subsidence is expected as the dense lithosphere in the roots of mountains pulls them down in the lead-up to delamination (Magni and Király, 2020), but how the required volume of negatively buoyant material can accumulate in such a short time is unclear.

Finally, dripping, usually defined as spheric 'blobs' of CC and mantle lithosphere that drip from the base of the crust (Fig. S4D), can also result in the loss of dense lower crust into the mantle. The validity of the dripping hypothesis can be tested by calculating the size of the sinking blob. The value obtained for a sphere-shaped crustal drip, based on a radius of 46 km (Supplementary Material), which is derived from a terminal velocity of 30 km/Myr in the upper mantle (Hafkenscheid et al., 2006), is 0.4 $\times$ 10^6 km^3. Around 150 to 230 drips would be required to account for the calculated crustal loss during the Himalayan orogen. This is inconsistent with the observed discrete stages of mountain uplift as shown in Fig. 5B, suggesting that dripping is unlikely to be the primary mechanism for the orogenic loss in the Himalaya-Tibetan Plateau.

4.3. Implication for climate changes

The rapid topographic uplift resulting from the foundering and detachment of the lower continental lithosphere in the Himalaya-Tibetan Plateau has implications for climate change. The elevation increase at ca. 24–20 Ma in southern Tibet (Fig. 5B), corresponds with the onset of intensified monsoonal rainfall in southern Asia at ca. 22 Ma, as indicated by the depletion of $\delta^{18}O$ in fossil teeth from the Himalayan Foreland Basin (Fig. 5C). Other geological evidence supporting the rapid uplift at this time includes a step increase in sediment accumulation rate from 30–24 Ma to 24–17 Ma in Bengal, Indus, and central Asian basins (Métivier et al., 1999), and rapid exhumation at ca. 25 Ma based on (U/Th)/He and fission track analyses in apatite and zircon in eastern Tibet (Wang et al., 2012). Uplift of the Himalaya-Tibetan Plateau in the late Oligocene, especially in the southern part, may have acted as a barrier, preventing warm moist air from the south from mixing with cool dry air from the north, leading to enhanced monsoon rainfall in southern Asia (Boos and Kuang, 2010). Here, rapid uplift is interpreted as a direct physical consequence of the periodic detachment of the lower CC and underlying mantle lithosphere, as suggested by the formation of the shoshonitic-adakitic magmatism in the southern Lhasa terrane (Fig. 5A), contrasting with the continuous subduction of CC and dripping hypotheses for orogenic loss.

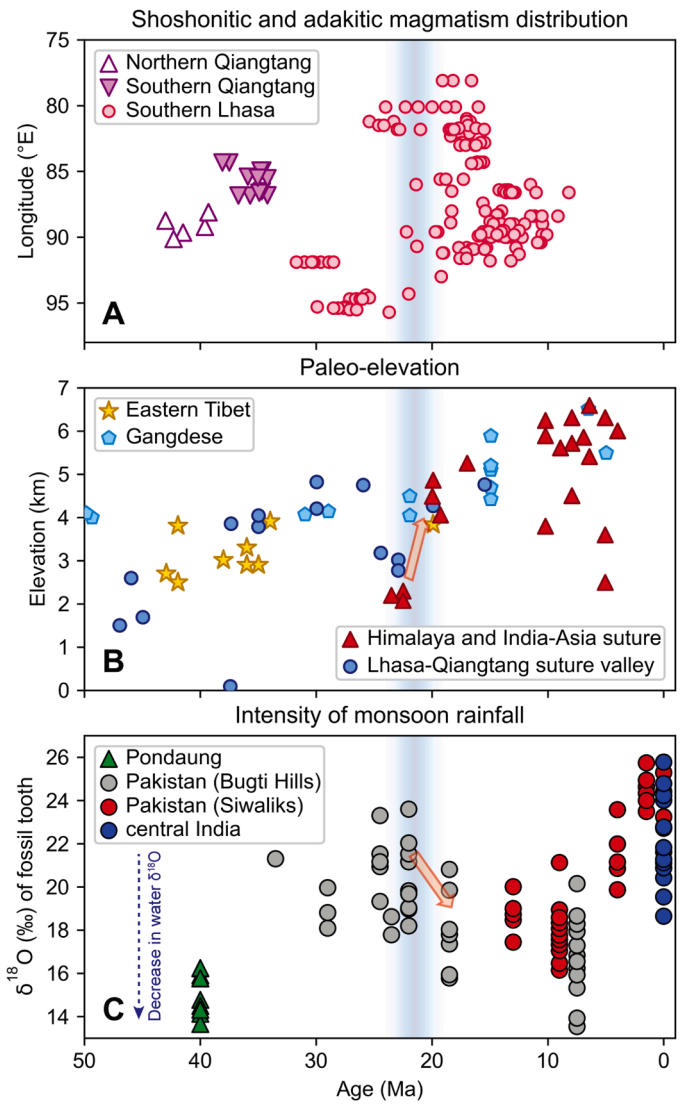

Fig. 5. (A) Spatial distribution of high-potassic and adakitic rocks in the southern Lhasa (Zhang et al., 2014), southern Qiangtang (Xu et al., 2023), and northern Qiangtang (Zeng et al., 2021) terranes. (B) Variations of paleo-elevation across the Himalaya-Tibetan Plateau, with most data points constrained by oxygen isotopes (Ding et al., 2022). (C) $\delta^{18}O$ values of fossil tooth analyses from the Middle Eocene Pondaung Formation from Myanmar and the younger Himalayan Foreland Basin from Pakistan and central India (Licht et al., 2014). The depletion of $\delta^{18}O$ is attributed to intense monsoonal rainfall. The shaded blue band represents the period (24–20 Ma) of rapid elevation increase in southern Tibet, which coincides with the onset of extensive shoshonitic-adakitic magmatism in the southern Lhasa terrane and strong monsoonal rainfall in the south of the Himalaya-Tibetan orogen.

Interestingly, the depletion in $\delta^{18}O$ with strong seasonality in fossil teeth from Myanmar at ca. 40 Ma, seen in Fig. 5C, indicates the existence of an older Asian monsoon (Licht et al., 2014), and it coincides with an earlier phase of shoshonitic-adakitic magmatism in the Qiangtang terrane at ca. 42–35 Ma (Fig. 5A). This magmatic activity has been linked to an early phase of lower lithosphere removal (Chung et al., 1998; Zeng et al., 2021), which is expected to lead to surface uplift. The uplift of the central plateau to near its modern elevation by ca. 40 Ma is supported by stratigraphic and fission-track studies (Wang et al., 2008). However, the exact timing and extent of the elevation increase, in response to the late Eocene delamination event, remains unclear from the oxygen isotope-based paleo-elevation record due to limited data (Fig. 5B).

4.4. Implication for mantle geochemistry

A second implication is the potential return of the delaminated lithosphere in mantle-derived melts, a process long promoted by the mantle plume paradigm. The delaminated lower crust and the concomitant SCLM could explain the trace element and isotopic features of some oceanic island basalts (OIB), such as the enriched-mantle-I (EM-I) end-member (Willbold and Stracke, 2010). Our calculations of orogenic loss suggest that a large amount of CC, which is (60–100) $\times 10^6$ km^3 in total for the three examined Cenozoic continent-continent collisions, has been recycled into the mantle. This crustal material and SCLM would take time to sink to the core-mantle boundary and resurface through plumes. For the modern mountain ranges evaluated here, the timescales are insufficient to account for the exotic crustal components in modern OIBs, as it would require >100 Myr for detached material to sink through the lower mantle with a free sinking rate of 20 km/Myr (Hafkenscheid et al., 2006). However, lower crust and SCLM, delaminated from ancient high Himalaya-like mountains, would have had the time required to sink to the core-mantle boundary, acquire the required heat, and return to the upper mantle in plumes. Zhu et al. (2022) have identified two periods of widespread high mountains, comparable to the modern Himalayas: Transgondwana Supermountain (650–500 Ma) and Nuna Supermountains (2.0–1.8 Ga), based on the temporal distribution of peak metamorphic pressures and high-pressure detrital zircons. The detachment of lower lithosphere during the formation of the austral Transgondwana Supermountain is geographically consistent with the OIBs with enriched geochemical signatures primarily found in the southern hemisphere (Jackson and Macdonald, 2022). Furthermore, we suggest that the detached eclogitised lower crustal roots of the Nuna Supermountains, are also a plausible source for the geochemical characteristics of some 'crust-contaminated' mantle plumes and had sufficient mantle-residence time of ca. 2 Gyr for the radiogenic isotopes to evolve to their observed values (Hart, 1984).

5. Conclusions

1) Our volume/mass balance calculations suggest that at least 30% of the shortened crust has been lost to the mantle (orogenic loss), during the India-Asia collision that formed the Himalaya-Tibetan Plateau, which exceeds the crust lost by surficial erosion by a factor of at least 2. The results agree well with previous studies. The primary mechanism for orogenic loss in the Himalaya-Tibetan Plateau is rapid foundering or detachment (delamination) of dense lower lithosphere (eclogitic lower crust and lithospheric mantle). This is supported by periodic paleo-elevation changes and episodic shoshonitic-adakitic magmatism.
2) Assuming a simple Airy-type isostatic model and that the orogenic loss in the Himalaya-Tibetan Plateau is due to delamination, the calculated elevation increase (2.1 km), derived from the average thickness of the delaminated block (20.4 km), agrees with the uplift history in the paleo-elevation record. The rapid uplift in the late Oligocene is supported by increases in sediment accumulation rates and exhumation records. This rapid uplift can be linked to the onset of intense monsoonal rainfall at ca. 22 Ma in southern Asia.
3) Our calculated lost crust, as a percentage of the overall shortened crust for the European Alps, ranges from around 15% to 50%, depending on the estimates of the initial crustal thickness and eroded volume taken from the literature. This orogenic loss is likely due to the subduction of lower CC, as imaged by seismic tomographic studies of the subducting European (and/or Adrian) lower lithosphere.
4) Our quantified orogenic loss of 30–64% for the Zagros Mountains, may result from a combination of mechanisms such as entrainment of continental passive margin with the detached oceanic lithosphere, continental subduction, and dripping.

5) Extending the concept of orogenic loss to the geological past suggests that the return of delaminated lithosphere from ancient high mountains like the Nuna (2.0–1.8 Ga) and Gondwana (650–500 Ma) supermountains can explain the enriched geochemical (EM-I) signatures observed in some oceanic basalts.

CRediT authorship contribution statement

Ziyi Zhu: Conceptualization, Methodology, Investigation, Visualization, Writing – original draft. **Zefeng Li:** Conceptualization, Methodology, Writing – review & editing. **Ian H. Campbell:** Investigation, Writing – review & editing. **Peter A. Cawood:** Investigation, Writing – review & editing, Funding acquisition. **Neng Lu:** Methodology, Writing – review & editing. **Oliver Nebel:** Writing – review & editing.

Declaration of competing interest

The authors declare no competing interests.

Acknowledgements

We are grateful to Roberto Weinberg for providing his insights into the Himalayan geology, Fabio Capitanio for sharing his knowledge of the Himalayan geodynamics, Sandy Cruden for guidance on calculating drip sizes, Andy Tomkins for discussion about delamination, and the two anonymous reviewers for their constructive comments. Comments from Walter Mooney and Fabio Capitanio on an earlier draft are also greatly appreciated. This study was supported by the Australian Research Council (grant FL160100168 to PAC).

Supplementary materials

Supplementary material associated with this article can be found, in the online version, at doi:10.1016/j.epsl.2024.119070.

Data availability

We have shared a separate data file (Supplementary Tables.xlsx) and a link to codes in the manuscript.

References

Aitchison, J.C., Ali, J.R., Davis, A.M., 2007. When and where did India and Asia collide? J. Geophys. Res.: Solid Earth 112.
Amante, C., Eakins, B.W., 2009. ETOPO1 arc-minute global relief model: procedures, data sources and analysis.
Bird, P., 1979. Continental delamination and the Colorado Plateau. J. Geophys. Res.: Solid Earth 84, 7561–7571.
Blanchette, A.R., Klemperer, S., Mooney, W.D., Zahran, H.M., 2020. Thickness of the Saudi Arabian crust.
Boos, W.R., Kuang, Z., 2010. Dominant control of the South Asian monsoon by orographic insulation versus plateau heating. Nature 463, 218–222.
Campbell, I.H., Stepanov, A.S., Liang, H.-Y., Allen, C.M., Norman, M.D., Zhang, Y.-Q., Xie, Y.-W., 2014. The origin of shoshonites: new insights from the Tertiary high-potassium intrusions of eastern Tibet. Contribut. Mineral. Petrol. 167, 1–22.
Capitanio, F., Morra, G., Goes, S., Weinberg, R., Moresi, L., 2010. India–Asia convergence driven by the subduction of the Greater Indian continent. Nat. Geosci. 3, 136–139.
Cawood, P.A., Hawkesworth, C., Dhuime, B., 2013. The continental record and the generation of continental crust. Bulletin 125, 14–32.
Chung, S.-L., Chu, M.-F., Ji, J., O'Reilly, S.Y., Pearson, N., Liu, D., Lee, T.-Y., Lo, C.-H., 2009. The nature and timing of crustal thickening in Southern Tibet: geochemical and zircon Hf isotopic constraints from postcollisional adakites. Tectonophysics 477, 36–48.
Chung, S.-L., Lo, C.-H., Lee, T.-Y., Zhang, Y., Xie, Y., Li, X., Wang, K.-L., Wang, P.-L., 1998. Diachronous uplift of the Tibetan plateau starting 40? Myr ago. Nature 394, 769–773.
Clift, P.D., Vannucchi, P., Morgan, J.P., 2009. Crustal redistribution, crust–mantle recycling and Phanerozoic evolution of the continental crust. Earth-Sci. Rev. 97, 80–104.
Curray, J.R., Emmel, F.J., Moore, D.G., 2002. The Bengal Fan: morphology, geometry, stratigraphy, history and processes. Mar. Pet. Geol. 19, 1191–1223.
Darin, M.H., Umhoefer, P.J., 2022. Diachronous initiation of Arabia–Eurasia collision from eastern Anatolia to the southeastern Zagros Mountains since middle Eocene time. Int. Geol. Rev. 64, 2653–2681.
Dewey, J., Hempton, M., Kidd, W., Saroglu, F., Şengör, A., 1986. Shortening of Continental Lithosphere: the Neotectonics of Eastern Anatolia—A Young Collision Zone, 19. Geological Society, London, pp. 1–36. Special Publications.
Ding, L., Kapp, P., Cai, F., Garzione, C.N., Xiong, Z., Wang, H., Wang, C., 2022. Timing and mechanisms of Tibetan Plateau uplift. Nat. Rev. Earth Environ. 3, 652–667.
England, P., Houseman, G., 1989. Extension during continental convergence, with application to the Tibetan Plateau. J. Geophys. Res.: Solid Earth 94, 17561–17579.
Gavillot, Y., Axen, G.J., Stockli, D.F., Horton, B.K., Fakhari, M.D., 2010. Timing of Thrust Activity in the High Zagros Fold-Thrust Belt, Iran, from (U-Th)/He thermochronometry. Tectonics 29.
Giese, P., 2005. Moho discontinuity, in: Selley, R.C., Cocks, L.R.M., Plimer, I.R. (Eds.), Encyclopedia of Geology. Elsevier, Oxford, pp. 645–659.
Guillot, S., Garzanti, E., Baratoux, D., Marquer, D., Mahéo, G., de Sigoyer, J., 2003. Reconstructing the total shortening history of the NW Himalaya. Geochem. Geophys. Geosyst. 4.
Gvirtzman, Z., Faccenna, C., Becker, T.W., 2016. Isostasy, flexure, and dynamic topography. Tectonophysics 683, 255–271.
Hafkenscheid, E., Wortel, M., Spakman, W., 2006. Subduction history of the Tethyan region derived from seismic tomography and tectonic reconstructions. J. Geophys. Res.: Solid Earth 111.
Handy, M.R., Schmid, S.M., Bousquet, R., Kissling, E., Bernoulli, D., 2010. Reconciling plate-tectonic reconstructions of Alpine Tethys with the geological–geophysical record of spreading and subduction in the Alps. Earth-Sci. Rev. 102, 121–158.
Hart, S.R., 1984. A large-scale isotope anomaly in the Southern Hemisphere mantle. Nature 309, 753–757.
Hatzfeld, D., Molnar, P., 2010. Comparisons of the kinematics and deep structures of the Zagros and Himalaya and of the Iranian and Tibetan plateaus and geodynamic implications. Rev. Geophys. 48.
Hu, X., Garzanti, E., Wang, J., Huang, W., An, W., Webb, A., 2016. The timing of India-Asia collision onset–Facts, theories, controversies. Earth-Sci. Rev. 160, 264–299.
Ingalls, M., Rowley, D.B., Currie, B., Colman, A.S., 2016. Large-scale subduction of continental crust implied by India–Asia mass-balance calculation. Nat. Geosci. 9, 848–853.
Jackson, M.G., Macdonald, F., 2022. Hemispheric geochemical dichotomy of the mantle is a legacy of austral supercontinent assembly and onset of deep continental crust subduction. AGU Adv. 3 e2022AV000664.
Kästle, E.D., Rosenberg, C., Boschi, L., Bellahsen, N., Meier, T., El-Sharkawy, A., 2020. Slab break-offs in the Alpine subduction zone. Int. J. Earth Sci. 109, 587–603.
Kay, R.W., Kay, S.M., 1991. Creation and destruction of lower continental crust. Geologische Rundschau 80, 259–278.
Kay, R.W., Kay, S.M., 1993. Delamination and delamination magmatism. Tectonophysics 219, 177–189.
Kearey, P., Klepeis, K.A., Vine, F.J., 2009. Global Tectonics. John Wiley & Sons.
Kuhlemann, J., Frisch, W., Dunkl, I., Székely, B., 2001. Quantifying tectonic versus erosive denudation by the sediment budget: the Miocene core complexes of the Alps. Tectonophysics 330, 1–23.
Lamb, S., Moore, J.D., Perez-Gussinye, M., Stern, T., 2020. Global whole lithosphere isostasy: implications for surface elevations, structure, strength, and densities of the continental lithosphere. Geochem. Geophys. Geosyst. 21 e2020GC009150.
Laske, G., Masters, G., Ma, Z., Pasyanos, M., 2013. Update on CRUST1. 0—A 1-degree global model of Earth's crust, Geophysical research abstracts. EGU General Assembly 2658.
Le Pichon, X., Fournier, M., Jolivet, L., 1992. Kinematics, topography, shortening, and extrusion in the India-Eurasia collision. Tectonics 11, 1085–1098.
Lee, C.-T.A., Thurner, S., Paterson, S., Cao, W., 2015. The rise and fall of continental arcs: interplays between magmatism, uplift, weathering, and climate. Earth Planet. Sci. Lett. 425, 105–119.
Leloup, P.H., Lacassin, R., Tapponnier, P., Schärer, U., Zhong, D., Liu, X., Zhang, L., Ji, S., Trinh, P.T., 1995. The Ailao Shan-Red river shear zone (Yunnan, China), tertiary transform boundary of Indochina. Tectonophysics 251, 3–84.
Li, C., Van der Hilst, R.D., Meltzer, A.S., Engdahl, E.R., 2008. Subduction of the Indian lithosphere beneath the Tibetan Plateau and Burma. Earth Planet. Sci. Lett. 274, 157–168.
Licht, A., Van Cappelle, M., Abels, H.A., Ladant, J.-B., Trabucho-Alexandre, J., France-Lanord, C., Donnadieu, Y., Vandenberghe, J., Rigaudier, T., Lécuyer, C., 2014. Asian monsoons in a late Eocene greenhouse world. Nature 513, 501–506.
Linzer, H.-G., Decker, K., Peresson, H., Dell'Mour, R., Frisch, W., 2002. Balancing lateral orogenic float of the Eastern Alps. Tectonophysics 354, 211–237.
Lippitsch, R., Kissling, E., Ansorge, J., 2003. Upper mantle structure beneath the Alpine orogen from high-resolution teleseismic tomography. J. Geophys. Res.: Solid Earth 108.
Lustrino, M., 2005. How the delamination and detachment of lower crust can influence basaltic magmatism. Earth-Sci. Rev. 72, 21–38.
Magni, V., Király, Á., 2020. Delamination.
McKenzie, D., Priestley, K., 2016. Speculations on the formation of cratons and cratonic basins. Earth Planet. Sci. Lett. 435, 94–104.
McQuarrie, N., van Hinsbergen, D.J., 2013. Retrodeforming the Arabia-Eurasia collision zone: age of collision versus magnitude of continental subduction. Geology 41, 315–318.
Métivier, F., Gaudemer, Y., Tapponnier, P., Klein, M., 1999. Mass accumulation rates in Asia during the Cenozoic. Geophys. J. Int. 137, 280–318.
Mooney, W.D., Barrera-Lopez, C., Suárez, M.G., Castelblanco, M.A., 2023. Earth crustal model 1 (ECM1): a 1×1 global seismic and density model. Earth-Sci. Rev., 104493

Mouthereau, F., Lacombe, O., Vergés, J., 2012. Building the Zagros collisional orogen: timing, strain distribution and the dynamics of Arabia/Eurasia plate convergence. Tectonophysics 532, 27–60.
Nábělek, J., Hetényi, G., Vergne, J., Sapkota, S., Kafle, B., Jiang, M., Su, H., Chen, J., Huang, B.-S., Team, t.H.-C., 2009. Underplating in the Himalaya-Tibet collision zone revealed by the Hi-CLIMB experiment. Science 325, 1371–1374.
Parsons, A.J., Hosseini, K., Palin, R.M., Sigloch, K., 2020. Geological, geophysical and plate kinematic constraints for models of the India-Asia collision and the post-Triassic central Tethys oceans. Earth-Sci. Rev. 208, 103084.
Paul, A., Hatzfeld, D., Kaviani, A., Tatar, M., Péquegnat, C., 2010. Seismic Imaging of the Lithospheric Structure of the Zagros Mountain Belt (Iran). Geological Society, 330. Special Publications, London, pp. 5–18.
Pirouz, M., Avouac, J.-P., Gualandi, A., Hassanzadeh, J., Sternai, P., 2017a. Flexural bending of the Zagros foreland basin. Geophys. J. Int. 210, 1659–1680.
Pirouz, M., Avouac, J.-P., Hassanzadeh, J., Kirschvink, J.L., Bahroudi, A., 2017b. Early Neogene foreland of the Zagros, implications for the initial closure of the Neo-Tethys and kinematics of crustal shortening. Earth Planet. Sci. Lett. 477, 168–182.
Replumaz, A., Negredo, A.M., Guillot, S., Van der Beek, P., Villaseñor, A., 2010. Crustal mass budget and recycling during the India/Asia collision. Tectonophysics 492, 99–107.
Rudnick, R.L., 1995. Making continental crust. Nature 378, 571.
Sánchez, L., Völksen, C., Sokolov, A., Arenz, H., Seitz, F., 2018. Present-day surface deformation of the Alpine region inferred from geodetic techniques. Earth Syst. Sci. Data 10, 1503–1526.
Schlunegger, F., Kissling, E., 2022. Slab load controls beneath the Alps on the source-to-sink sedimentary pathways in the Molasse basin. Geosci. (Basel) 12, 226.
Schmid, S.M., Pfiffner, O.-A., Froitzheim, N., Schönborn, G., Kissling, E., 1996. Geophysical-geological transect and tectonic evolution of the Swiss-Italian Alps. Tectonics 15, 1036–1064.
Sinclair, H., 1997. Tectonostratigraphic model for underfilled peripheral foreland basins: an Alpine perspective. Geol. Soc. Am. Bull. 109, 324–346.
Su, H., Zhou, J., 2020. Timing of Arabia-Eurasia collision: constraints from restoration of crustal-scale cross-sections. J. Struct. Geol. 135, 104041.
Talebian, M., Jackson, J., 2002. Offset on the main recent fault of NW Iran and implications for the late cenozoic tectonics of the Arabia–Eurasia collision zone. Geophys. J. Int. 150, 422–439.
Van Hinsbergen, D.J., Lippert, P.C., Dupont-Nivet, G., McQuarrie, N., Doubrovine, P.V., Spakman, W., Torsvik, T.H., 2012. Greater India Basin hypothesis and a two-stage Cenozoic collision between India and Asia. Proceed. Natl. Acad. Sci. 109, 7659–7664.
van Hinsbergen, D.J., Lippert, P.C., Huang, W., 2017. Unfeasible subduction? Nat. Geosci. 10, 878–879.
van Hinsbergen, D.J., Steinberger, B., Doubrovine, P.V., Gassmöller, R., 2011. Acceleration and deceleration of India-Asia convergence since the Cretaceous: roles of mantle plumes and continental collision. J. Geophys. Res.: Solid Earth 116.
Vance, D., Bickle, M., Ivy-Ochs, S., Kubik, P.W., 2003. Erosion and exhumation in the Himalaya from cosmogenic isotope inventories of river sediments. Earth Planet. Sci. Lett. 206, 273–288.
Wang, C., Zhao, X., Liu, Z., Lippert, P.C., Graham, S.A., Coe, R.S., Yi, H., Zhu, L., Liu, S., Li, Y., 2008. Constraints on the early uplift history of the Tibetan Plateau. Proceed. Natl. Acad. Sci. 105, 4987–4992.
Wang, E., Kirby, E., Furlong, K.P., Van Soest, M., Xu, G., Shi, X., Kamp, P.J., Hodges, K., 2012. Two-phase growth of high topography in eastern Tibet during the Cenozoic. Nat. Geosci. 5, 640–645.
White, W.M., 2015. Isotopes, DUPAL, LLSVPs, and anekantavada. Chem. Geol. 419, 10–28.
Willbold, M., Stracke, A., 2010. Formation of enriched mantle components by recycling of upper and lower continental crust. Chem. Geol. 276, 188–197.
Xu, W., Weinberg, R.F., Tian, S.H., Hou, Z.Q., Yang, Z.S., Chen, L., Lai, F., 2023. K-Rich Adakite-Like Rocks in Central Tibet: fractional Crystallization of a Hydrous. Alkaline Primit. Melt. Geophys. Res. Lett. 50 e2022GL099887.
Zeng, Y., Ducea, M.N., Xu, J., Chen, J., Dong, Y.-H., 2021. Negligible surface uplift following foundering of thickened central Tibetan lower crust. Geology 49, 45–50.
Zhang, L.-Y., Ducea, M.N., Ding, L., Pullen, A., Kapp, P., Hoffman, D., 2014. Southern Tibetan Oligocene–Miocene adakites: a record of Indian slab tearing. Lithos 210, 209–223.
Zhang, W., Jiménez-Munt, I., Torne, M., Vergés, J., Bravo-Gutiérrez, E., Negredo, A.M., Carminati, E., García-Castellanos, D., Fernàndez, M., 2022. Geophysical-petrological model for bidirectional mantle delamination of the Adria microplate beneath the northern Apennines and Dinarides orogenic systems. J. Geophys. Res.: Solid Earth 127, e2022JB024800.
Zhu, D.C., Wang, Q., Cawood, P.A., Zhao, Z.D., Mo, X.X., 2017. Raising the Gangdese mountains in southern Tibet. J. Geophys. Res.: Solid Earth 122, 214–223.
Zhu, Z., Campbell, I.H., Allen, C.M., Brocks, J.J., Chen, B., 2022. The temporal distribution of Earth's supermountains and their potential link to the rise of atmospheric oxygen and biological evolution. Earth Planet. Sci. Lett. 580, 117391.